Surface enhanced Raman scattering (SERS)-active bacterial detection by layer-by-layer (LbL) assembly all-nanoparticle microcapsules

Jie Li,[a] Dmitry Khalenkow,[a] Dmitry Volodkin,[b] Ales Lapanje,[c] Andre G. Skirtach,[a] and Bogdan V. Parakhonskiy[a]

a) Bio-Nanotechnology Laboratory, Faculty of Bioscience Engineering, Ghent University, 9000 Ghent, Belgium

b) Department of Chemistry and Forensics, School of Science and Technology, Nottingham Trent University, Clifton Lane, Nottingham NG11 8NS, UK

c) Department of Environmental Sciences, Jozef Stefan Institute, Jamova cesta 39, 1000 Ljubljana, Slovenia

Corresponding author's E-mail: jiejieli.li@ugent.be

ABSTRACT: Polymeric microcapsules composed by the layer-by-layer (LbL) approach have been used for various applications including drug delivery into cells and *in vivo*, conducting enzyme catalyzed reactions, performing sensoric functions. Typically, LbL-assembled microcapsules have been formulated via alternating deposition of positively and negatively charged polyelectrolytes onto sacrificial templates or so-called cores. In this work, we extend the LbL assembly to produce microcapsules solely based on nanoparticles instead of polymers. Both gold and silver nanoparticles have been deposited as oppositely charged layers in the LbL assembly. We have identified that 5 layers of nanoparticles is the minimum number of layers for a stable assembly of capsules on calcium carbonate templates. Subsequently, the composite capsules comprised of nanoparticles were applied as Surface Enhanced Raman Scattering (SERS) platform, where the nanoparticle-based shell of capsules is shown to enable SERS of both solutes and macromolecular structures such as bacterial cells.

Graphical Abstract

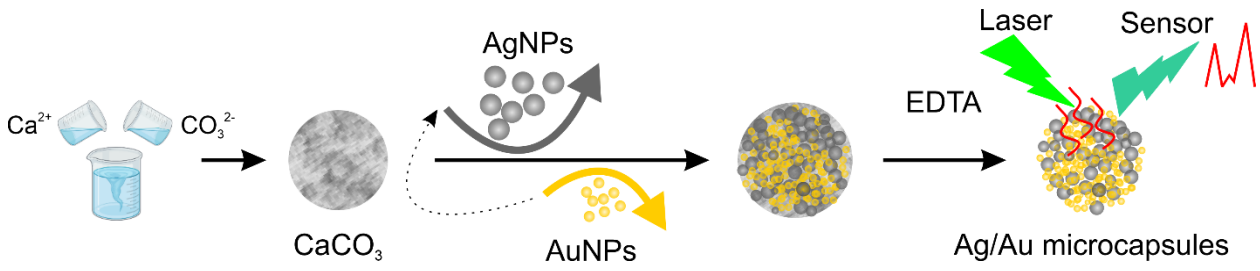

Keywords: polyelectrolyte, multilayer, LbL, capsules, SERS, bacterial

1. Introduction

In the recent years, application of polymeric micro- and nano- capsules has been steadily growing. In the general area of polymeric microcapsules, those assembled by the layer-by-layer (LbL) technique are particularly interesting due to flexibility of their design and a variety of stimuli, which can be used for controlling their assembly and their properties.[1–3]

The LbL capsules have been introduced in the late 90-ies, while subsequently, encapsulation methods have been developed, including pH-based method,[4] temperature-based method,[5] encapsulation into templates,[6,7] while pH-based method is also used in the presence of enzymes (biodegradability).[8–10] In many applications, the shell of capsules and even cells is functionalized with nanoparticles, which could serve as "hot spots" for absorbing the respective external stimuli such as electromagnetic light waves in the case of laser-based release,[11–14] magnetic fields in the case of magnetic field-based activation,[15] and sound waves in the case of ultrasound.[16] In initially demonstrated release using ultrasound very high ultrasound intensities were used.[17] But substantial progress has taken place and the intensities necessary for microcapsule activation and opening substantially decreased.[18] An essential reduction of necessary ultrasound intensity was achieved by adsorbing or synthetizing in situ nanoparticles in the shell of polymeric capsules, for example, SiO_2 nanoparticles on the capsule shells.[19,20]

Nanoparticles have been already incorporated into the layers of microcapsules,[21] but the assembly was mainly done sequentially with polymers.[22–29] LbL layers of alternative deposition of SiO_2 and TiO_2 nanoparticles has led to effective antireflection coatings, but SiO_2 were used as stacks for essentially smaller TiO_2 nanoparticles.[30] Nanoparticle adsorption on the surfaces has resulted to an enhanced surface plasmon Raman resonance enhancement.[28,31–34] Meanwhile different interfaces, where nanoparticles were used as surfactants have also been

considered by B. Binks.[35] Using solely nanoparticles as surfactants to build novel nanoscale platform has been reported by M. Haase[36] via oil-in-water emulsion approach. Developing a novel solely nanoparticle-based approach to capsule preparation would be promising in different fields such as those where the presence of polymers is either not required or even can or should be avoided.

Polyelectrolyte multilayer capsules have become powerful tools for different biomedical applications including drug delivery, theranostic and biosensing.[37] Especially, sensor and bio-sensor related applications have been used for different,[38] so it would be logical to aim developing a sensor based on capsules for detection of molecules. One candidate for such sensor-mechanisms involving nanoparticles is Surface-Enhanced Raman Scattering (SERS), where the fields, and as a result, scattering by molecules, is amplified due to plasmonic effect on nanoparticles.

It is very promising to design the carrier with a dual even multiple functionality such as: delivery function, sensorics function and theranostics[39]. For this reason the functionalization of the carrier with plasmonic nanoparticles on the shell could provide the detection function for such carrier.[40] For example, among these reported lectures, silver and gold nanoparticles were common involved as enhancers.[41–43]

Various functionalized porous carriers, such as calcium carbonate porous template,[44–46] hydroxyapatite[47] and silica particles[48], will enhance the detection ability by 6 order of magnitude. Other than the porous carrier the polymeric capsules with as a SERS platform also developed. Polyelectrolyte capsules[38] and the alginate hydrogel capsules[49] demonstrate possibility not only release substance under the ultrasound but also provide the amplification inside the *C-elegance*[50]. The microcapsules made of polymeric and metallic nanoparticles are also

suitable for performing label-free detection by SERS micro-spectroscopy.[51,52] In another study,[53] RNA detection using polymeric microcapsules with encapsulated gold nanoparticles has been made and presented. Furthermore, pH and carbamide sensing have been also realized using SERS.[54,55]

The colloidal and chemical instability of nanoparticles may lead to a decreased intensity of the received SERS signal,[56] while their controlled aggregation of nanoparticles[57] or waveguide design[58] allow for a significant enhancement of the SERS signal. Furthermore, new approaches for development of SERS-based diagnostic platforms are currently pursued, including waveguide-based designs[58] and fiber[59,60].

SERS platforms have been applied in different fields including: in cell biology[57,61,62] and biomolecules[53,63,64] and environment.[65,66] SERS detection of molecules using microcapsules represents a different approach compared to using nanoparticles alone for detection of molecules. This is particularly noticeable for detection of, for example, exosomes[67–69] and bacteria[70,71]. Meanwhile, accurate, fast, simple and sensitive method of detection of microorganisms, such as *Escherichia coli*, which is involved in nosocomial, waterborne and foodborne infectious diseases, are important for food safety and human health care.[72] Accordingly, there has always been a strong driving force to develop a rapid, simple, and efficient method for bacterial cell detection with SERS application.

Most of the microcapsules are hybrid, which contained organic and inorganic components. But the PEM microcapsules has a number of drawbacks such as material consuming and laborious process of synthesis, high permeability to small molecules, low reproducibility, aggregation and unknow long-term stability frequently using the synthetic polymers.[73] For this reason to design a novel

types of microcapsules based on inorganic components with capability to enhance the Raman signal still represents a significant challenge.

In this work, we have assembled one new type of microcapsules purely composed of nanoparticles in an aqueous solution. Sequential adsorption of silver and gold nanoparticles has been carried out, where silver nanoparticles were synthesized in situ, while gold nanoparticles have been added upon sequential build-up of the layers of silver/gold capsules. The LbL assembly of nanoparticles has been carried out on calcium carbonate templates, which were subsequently removed forming the hollow capsules comprised of nanoparticles. Scanning electron microscopy analysis has been performed to examine the capsule structure. The constructed capsules have been applied as a SERS platform which achieved rapid detection of standard molecules and microorganisms.

2. Materials and methods

2.1 Materials

Gold(III) chloride trihydrate ($HAuCl_4$, ≥99.9%), D-(+)-Glucose ($C_6H_{12}O_6$, 180.16 Da, ≥99.5%), Tetraoctylammonium bromide (TOAB, $[CH_3(CH_2)_7]_4N(Br)$, 98%), Toluene (99.8%), Sodium sulfate anhydrous (Na_2SO_4 ,>99.0%), 4-dimethylaminopyridine (DMAP, $C_7H_{10}N_2$, ≥99%), Sodium carbonate (Na_2CO_3, ≥99.5%), Calcium chloride ($CaCl_2$, ≥93.0%), Ammonium hydroxide solution (28.0-30.0% NH_3 basis), Silver nitrate ($AgNO_3$, >99%), Sodium borohydride ($NaBH_4$, 99%) and Rhodamine 6G (dye content ~95%, 479.01 Da) were purchased from Sigma-Aldrich. In all experiments, Milli-Q water with resistivity higher than 18.2 MΩ cm was used.

2.2 Particle Synthesis

Gold nanoparticles (AuNPs) were synthesized via the modified protocol of Gittins[74] as follows. 30 mL of 30 mM $HAuCl_4$ was added to 80 mL solution of 25 mM tetraethylammonium bromide in toluene. 25 mL freshly prepared $NaBH_4$ was added to the mixture and stirred for 30 min. After that, two phases were split and the organic phase was subsequently washed with 0.1 M H_2SO_4 0.1 M NaOH, and H_2O for three times, afterwards dried with anhydrous Na_2SO_4. Last, 0.1 M DMAP solution with a ratio of 1:1 was used to transfer AuNPs in prepared nanoparticle mixtures into aqueous solution.

Spherical calcium carbonate microparticle core was fabricated via a modified previous reported protocol.[75] 1 mL of Na_2CO_3 (0.33 M) was loaded into a 100 mL glass beaker, then an equal volume of $CaCl_2$ (0.33 M) was injected rapidly and stirred at 600 rpm for 1 min. The color of the

mixture solution became milky-white immediately after mixing. The synthesized $CaCO_3$ particles were carefully washed with 70% ethanol and dried for whole night at 100 °C.

5% $[Ag(NH_3)_2]OH$ solution, also known as Tollens' reagent, was obtained by adding 0.5 M ammonium hydroxide to 0.5 M $AgNO_3$ dropwise until the complex solution become transparent.

2.3 Capsule synthesis

To produce 4 bilayers silver and gold microcapsules, 10 mg of $CaCO_3$ microparticle powder was placed in a 2 mL Eppendorf tube and dissolved in 1 mL of deionized water. The classic silver mirror reaction[45] was conducted on the $CaCO_3$ core to form the first layer. A total of 200 µL of fresh Tollens' reagent and 200 µL D-glucose were injected into the tube and was left on stirring for one hour. After that, silver nanoparticle coated $CaCO_3$ microparticles were washed three times by water. After washing steps, 1 mL as-prepared AuNPs were added and stirred for 15 minutes for the fabrication of the next layer after 3 minutes of the ultrasound treatment. Wash the sediment and repeat with AuNPs for second layer until the supernatant shows red color to confirm the formation of nanoparticles. EDTA solution with a concentration of 0.2 M at pH 7 was added to remove the sacrificial $CaCO_3$ core. Further, excessive EDTA salt was removed by washing with deionized water several times.

2.4 Bacteria preparation and growth

For experiments with bacteria the strain of *Escherichia coli* TOP10 was used with genetic properties: F– mcrA Δ(mrr-hsdRMS-mcrBC) Φ80lacZΔM15 ΔlacX74 recA1 araD139 Δ(ara leu) 7697 galU galK rpsL (StrR) endA1 nupG. Bacterial suspension was obtained from the stationary overnight culture grown on NB1 medium (Carl Roth) at 37 ºC on a rotary shaker with preset at

150 rpm. To wash out the media components we centrifuged 50ml culture at 5000g for 5 min and resuspended in 30 mL sterile 0.9% NaCl or Milli-Q water. Washing was repeated 3 more times. Finally, cells were resuspended in 1ml and frozen at -20 ºC after addition of 10% glycerol. Before experiments, cells were thawed and washed one more time to wash out any cell debris as well as glycerol.

2.5 Scanning Electron Microscopy (SEM)

The morphology of the surface-modified particles and capsules both were examined in a scanning electron microscope (JEOL JSM 7100F SEM, JEOL Ltd., Japan). To study the fabrication process of the microcapsules, aliquots which own different quantity of layers for each type of microcapsules were taken for SEM.

2.6 X-Ray Diffraction (XRD)

The XRD patterns of the samples were recorded using a powder X-ray diffractometer (Rigaku MiniFlex, Rigaku Ltd., Japan) with Cu-Kα radiation (40 kV, 15 mA, NiCKβ-filter, 1.5406 Å) in the 2Θ angle range from 20 to 80° with a scanning step of 0.01° and a rate of 7°/min. Data were evaluated using the integrated X-ray powder diffraction software SmartLab Studio II and Database pdf4.

2.7 Raman Spectroscopy

Raman spectra were acquired on a Raman microscope (Alpha300, WiTec GmbH, Germany) with 785 nm NIR (near-infrared) laser. To test the performance of substrates for surface enhancement Raman spectroscopy (SERS), Rhodamine 6G water solution (10^{-3}, 10^{-4}, and 10^{-5} M) was used as an analyte. All SERS maps (30 × 25 μm) of R6G with concentrations of 10^{-3}, 10^{-4} and 10^{-5} M,

were recorded using a Nikon 40×/ 0.6 NA objective with laser power of 16 mW and integration time of 5 seconds per spectrum. Enhancement factors (EF) were calculated according to the formula:

$$EF = \frac{I_{SERS}}{I_{Raman}} \cdot \frac{p_{Raman}}{p_{SERS}} \cdot \frac{c_{Raman}}{c_{SERS}} \qquad (1)$$

where I_{SERS} and I_{Raman} are intensities of the SERS amplified signal and initial signal of the control analyte; p_{SERS} and p_{Raman} are laser power for SERS spectra and control analyte; c_{SERS} and c_{Raman} are the concentration of R6G for SERS spectra and the control analyte, respectively.

In prior of the acquisition of signals from Raman, suspension of *E. coli* cells was washed with 0.9% NaCl and Milli-Q water. The washed suspension of bacterial cells was pipetted on microcapsules and then SERS measurements were made on dried samples.

Enhancement factors for bacterial (EFB) were calculated according to the formula:

$$EFB = \frac{I_{SERS}}{I_{Raman}} \cdot \frac{p_{Raman}}{p_{SERS}} \qquad (2)$$

where I_{SERS} and I_{Raman} are intensities of the SERS amplified signal and initial signal of the control bacteria; p_{SERS} and p_{Raman} are laser power for SERS spectra and control bacteria, respectively.

2.8 Image analysis

Analysis of SEM and Raman images was done by using ImageJ software (http://rsb.info.nih.gov/ij/). SERS maps were chosen to count the capsules.

3. Results and discussion

The schematic of design and study of the inorganic Ag/Au capsules as SERS platform is highlighted in Scheme 1. In the first step, calcium carbonate templates for microcapsules are prepared. Calcium carbonate particles were chosen as templates because of their biocompatibility, easiness of preparation and controllable size, shape. For preparation of calcium carbonate particle templates, solutions containing the corresponding salts of $CaCl_2$ and Na_2CO_3 were poured into a beaker upon rigorous steering to fabricate porous calcium carbonate cores. SEM analysis (scheme 1b, c) showed that the obtained vaterite particles (4.01 ± 0.05 μm) with spherical shape contained 5 % of the calcite.

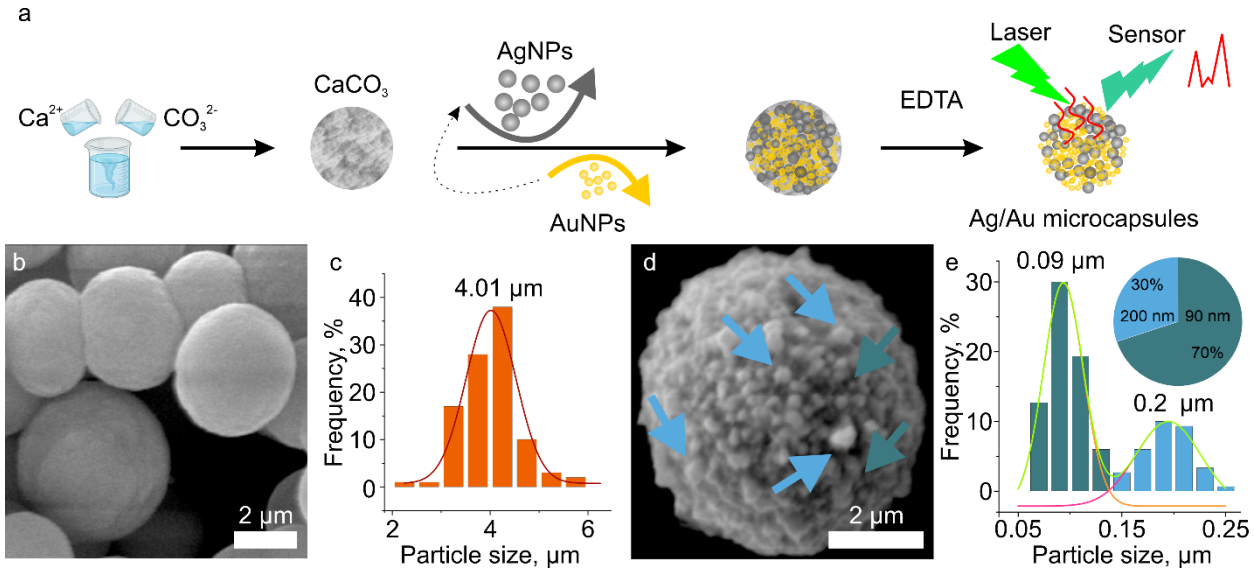

Scheme 1. Schematics of the experiment showing major steps employed for the preparation of all-nanoparticle capsules.

In the next step, the formation of the nanoparticle shell was performed. For this purpose, AgNPs and AuNPs were used, but they were prepared differently. AgNPs were obtained via an in-situ synthesis named silver-mirror reaction. Based on SEM (scheme 1d, e) analysis, we obtained that AgNPs with two main sizes (0.09 ± 0.02 μm and 0.20 ± 0.03 μm, R^2=0.9823) are present on the

surface, while the shape of both particles is almost spherical. This various size represent the synthesis in a surface and the size of the particles are limited by the porous size which are 90 nm of the calcium carbonate from other and number of the particles are formatted in solution and have a larger size up to 250nm average 200 nm.[75,76]

Such an approach represents an easy way of directly coating the surfaces of capsules as it was discussed earlier.[13] For an alternating layer in the LbL assembly, AuNPs were used. Although there are many ways for preparation of AuNPs, having a high concentration of nanoparticles is very important for an effective coverage of the surface of all particles.[77] That is why in the synthesis of AuNPs with size 6 nm we have chosen a method of AuNPs with a high yield (i.e. high concentrations) which are stabilized by 4-dimethylaminopyridine (DMAP). After the microcapsule assembly was complete, calcium carbonate templates on which the capsules formed were removed by EDTA producing microcapsules with nanoparticle on the walls.

The bilayer of AgNPs and AuNPs covers the surface of calcium carbonate particles until the core is completely covered with the increasing number of bilayers of AgNPs and AuNPs, as shown in Figure 1a-e. Meanwhile, most walls of capsules with 4 layers were destroyed when the template was removed, as it can be seen in Figure 1f. Note that the stable hollow microcapsule were obtained with the minimum of 5 layers of nanoparticles, as it is shown in Figure 1g, h, i and j. 5 layers is sufficient even though the gold particles are small (6 nm), they contribute to the shell stability as well. SEM images (Figure S1) can also show that there is no significant difference between the size of capsules with a diameter of approximately 4.1-4.3 μm (4.11± 0.96 μm, 4.38± 0.77 μm, 4.33± 0.67 μm, 4.28± 0.61 μm depended on the structure) compared with the size of the initial calcium carbonate cores 4.01 ± 0.05 μm.

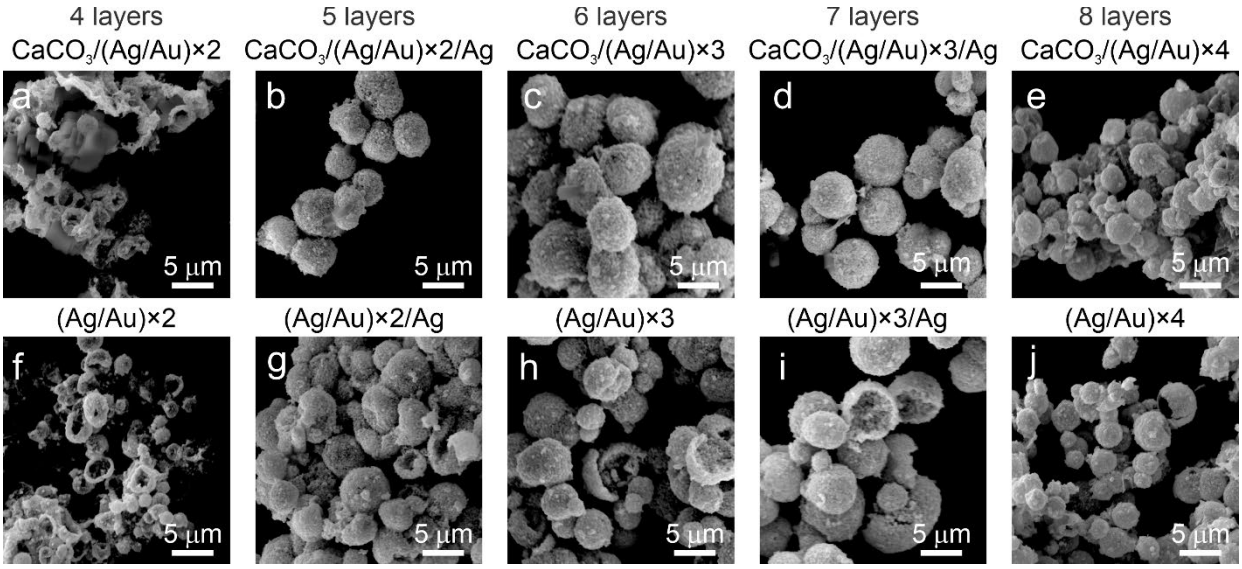

Figure 1. SEM images of calcium carbonate with adsorbed nanoparticles (top row a-e) and hollow capsules obtained after $CaCO_3$ dissolution (bottom row f-j) with different number of the metal nanoparticles layers: (a, f) 4 layers - (Ag/Au)×2 ; (b, g) 5 layers - (Ag/Au)×2/Ag ; (c, h) 6 layers- (Ag/Au)×3; (d, i) 7 layers - (Ag/Au)×3/Ag and (e, j) 8 layers - (Ag/Au)×4.

The efficient dissolution of calcium carbonate template was proved by the X-Ray diffraction (XRD) (Figure 2) processed via the Rietveld analysis. The samples with $CaCO_3$ core inside (Figure 2a) have one main peak (29.32°) assigned to the (104) plane and some feeble peaks, which correspond to calcite ($CaCO_3$) as well as the peak of silver and gold. All spectra of capsules with the dissolved $CaCO_3$ cores only have four main diffraction peaks at 38.03°, 44.20°, 64.29°, and 77.20° could are assigned to (111), (200), (220), and (311) planes of AgNPs, respectively (Figure 2b) and well-matched with the Database pdf4. It should be noted that the peaks at 38.05°, 44.22°, 64.32° and 77.24° could be also assigned to (111), (200), (220), and (311) planes of AuNPs (Figure 2b), which are challenging to distinguish from those of AgNPs. In addition, it was noticed that the vaterite core converted to calcite, this can be assigned to a long synthesis process in an aqueous solution. There are no calcium carbonate peaks found on XRD spectra of all samples obtained after

calcium carbonate dissolution (Figure 2b), which means that microcapsules were formed only by metal nanoparticles.

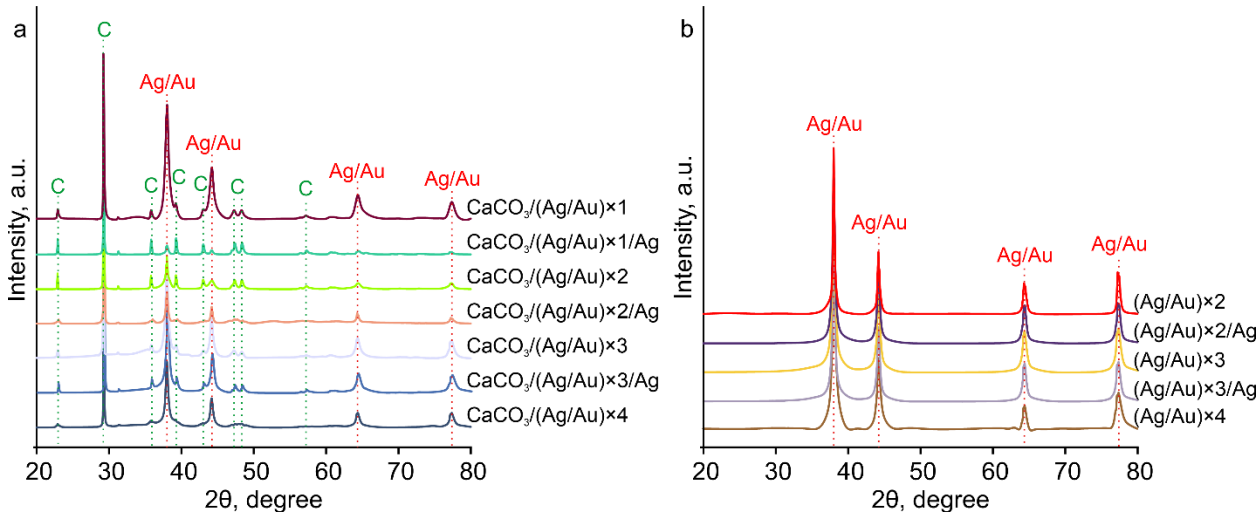

Figure 2. XRD diffraction spectra of (a) calcium carbonate core with adsorbed nanoparticles and (b) hollow all nanoparticle microcapsules synthesized with different composite structures: (Ag/Au)×2, (Ag/Au)×2/Ag, (Ag/Au)×3, (Ag/Au)×3/Ag, (Ag/Au)×4, respectively; where the red and green dash lines indicate silver/gold and calcite (C), respectively.

The SERS capability of Au/Ag microcapsules were tested by measuring R6G as a model analyte. The mechanism of adsorption of this molecule is the physical sorption on the surface of the scaffold. As the hollow microcapsules only could be obtained with at least 5 layers of nanoparticles, the effect of the concentrations of R6G on the SERS sensitivity Au/Ag microcapsules with 6 layers and 8 layers both were measured.

Prior acquiring SERS spectra, microcapsules were incubated in solution of R6G at different concentrations of 10^{-3}, 10^{-4}, 10^{-5} M for 20 min. Typically, R6G has the most intensive fingerprint peaks located at 1308 cm^{-1}, 1357 cm^{-1}, 1506 cm^{-1} representing the C-C aromatic stretching of the

dye (R6G), as it is shown in Figure 3. Peaks appearing in the spectrum at 1178 cm^{-1} and 795 cm^{-1} are due to the in-plane and out-plane bending of C−H, respectively, while the band at 1076 cm^{-1} can be assigned to residual calcium carbonate (Figure 3a).

To evaluate the efficiency of these microcapsules as a SERS platform, an analytical enhancement factor (EF) was calculated by applying eq 1 based on the intensity of the most intensive peak of 1506 cm^{-1} (Figure 3b). The microcapsules fabricated with AuNPs as the outermost layer only demonstrate amplification up to than 20 folds properties. This issue could be due to the organic stabilizer surrounding on AuNPs decrease the local conductivity of the metallic surface.

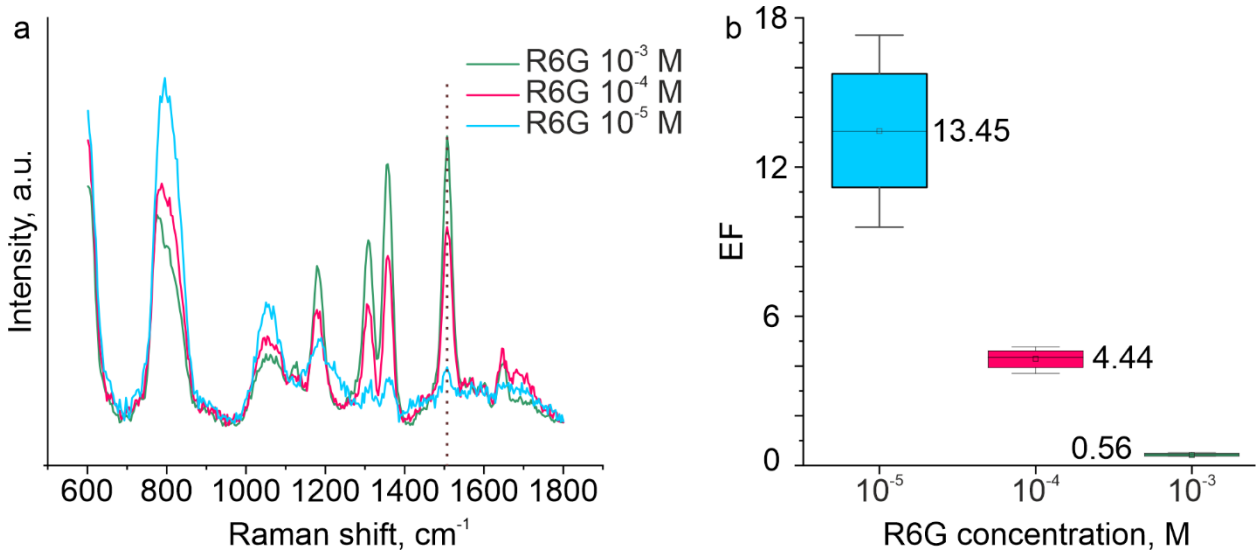

Figure 3. SERS spectra (a) and EF (b) based on the intensity of the peak of 1506 cm^{-1} for varying concentrations (10^{-3}, 10^{-4}, and 10^{-5} M) of R6G adsorbed by microcapsules with the shell comprising of (Ag/Au)×4. The mean value of the EF is shown near the corresponding boxes. Laser power: 120 mW.

To prove this concept, we studied the EF of 7 layer capsules possessing the following structure (Ag/Au)×3/Ag with non-stabilized AgNPs as the outermost layer. These microcapsules showed a

significant increase of amplification signals up to 10^7 at the lowest laser power (0.05 mW), as it is shown in Fig. 4a. It can be noted that two outliers appear when the laser power is 0.1 and 0.5 mW at the concentration of R6G of 10^{-4} M. These suggests that so-called “hot spots” contribute to the SERS signals enormously. We further calculated an enhancement factor based on the Raman intensity at 1506 cm^{-1} for all imaged areas (3*3=9 points), as shown in Fig. 4b. The EF calculated from three independent scanned area (Fig. 4b) could be seen on the scanned maps. EF did not show significant variation in the scanned area.

Such high amplification can be explained by the structure of the microcapsules shell that all nanoparticles of the in the shell touch each other. In this case, the optimal distance between nanoparticles and conductivity could be provided.[78,79]

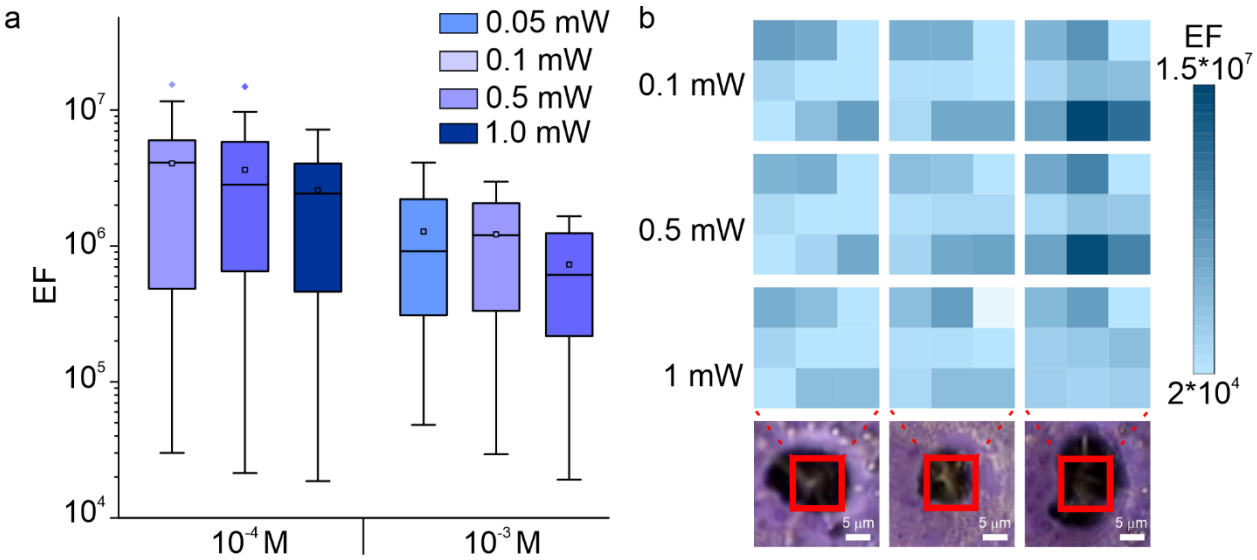

Figure 4. (a) EF of R6G adsorbed by microcapsules with shell of (Ag/Au)×3/Ag calculated on the different laser power (0.05 mW – 1 mW) showing a value range of 10^4-10^7. The left group was measured with R6G of 10^{-3} M, and right was measured with R6G of 10^{-4} M. Two pots out of the box are outliers. (b) EF map of R6G adsorbed by microcapsules with shell of (Ag/Au)×3/Ag from were calculated based on acquiring the Raman intensity and eq 1 at 1506 cm^{-1} from three independent areas (column from left to right) highlighted with the red square in optical microscopy images (bottom row) with various laser power (0.1 mW, 0.5 mW and 1 mW).

SERS detection of bacteria using microcapsules

For demonstrate the proof of principal using designed contains in biomedicine for detect the microorganisms such as bacteria we used model organism the *E. coli* strain. The SERS spectra for different power of laser (Fig. 5). Bacterial Raman spectra (blue line) shown in Fig. 5 consist of bands representing the cell contents, primarily proteins, lipids, carbohydrates, and nucleic acids.[80] For example, strong Raman peaks located at 1000 and 1659 cm^{-1} were assigned to

298 proteins,[81,82]; the peak at 1446 cm^{-1} was assigned to carbohydrates or lipids,[81,82] 1029; and
299 1128 cm^{-1} have been previously attributed to carbohydrates,[82,83] 721 cm^{-1} corresponds to
300 nucleic acids[82,83]. Table 1 shows the main Raman peaks of the three spectra and the tentative
301 assignment for the most relevant bands. It is observed that there is a significant SERS enhancement
302 at different laser power and a clear trend of variation of enhancement with increase in the laser
303 power between the range of 1000-1700 cm^{-1} in Fig. 5 (red and green line), while SERS
304 enhancements did not present enormous difference in this range.

305 On the other hand, there were more vibrational bands observed in SERS spectra of *E. coli*, which
306 depend on the power of laser. For example, peaks at 1190, 1399, 1503 cm^{-1} appear only in the
307 SERS spectra, can result in the high SERS signals. To use such platform to detect bacterial cells,
308 it is essential to estimate the enhancement factor for SERS signals. In this case, we used eq 2 based
309 on the most intensive SERS peak present at 1446 cm^{-1}, which corresponds to the CH_2 and CH_3
310 vibrations of proteins and lipids to count the EFB. The enhancement factor of *E. coli* was measured
311 to be up to 7.8×10^4 and 2.8×10^3 with laser power of 1.5 mW and 5 mW, respectively.

Table 1 Assignments of SERS signatures of *Escherichia coli* acquired from microcapsules and Raman bands of *Escherichia coli* taken from bacteria suspension in water based on recent literature. [80,82,84–88]

Peak position (cm^{-1})			Chemical groups assignment
Raman	SERS		
87 mW	1.5 mW	5 mW	
	621	619	CC twisting—tryptophan
	648	648	Tyrosine
	684	673	Valine
	706	710	Calcium Carbonate
	731	733	Adenine ring stretching; peptidoglycan
	749	749	Tryptophan
	781	781	Cytosine, uracil (ring stretching)
	796	799	C–O–P–O–C—RNA binding
825	842		Tyrosine
	878	874	CCH deformation (Agar)
	938	932	C–C stretching (amide III)—protein
	964	964	CCH deformation (Agar)
1000	988	988	C–C skeletal stretching of aromatic ring—phenylalanine/tyrosine
	1021		Bacteria metabolism (?)
	1056		Carbohydrates
1095	1083	1090	Nucleic acids (PO_2^-symmetrical stretching); C–C and C–O–C skeletal stretching—glycosidic linkage of saccharides
1121	1155		carbohydrates
	1190	1200	Amide III; C–C tyrosine stretching, phenylalanine, tryptophan (protein)
1248	1239	1248	C–N e N–H stretching (amide III); thymine and adenine (ring breathing); CH_2 lipids deformation; saccharides
1316	1281	1280	C–N and N–H stretching (amide III); CH_2 and CH_3 —protein deformation; guanine breathing ring
1330	1345	1355	CH_2 and CH_3 —fatty acids and protein deformation; N–H stretching (amide III); C–C stretching—tryptophan; adenine, guanine (ring breathing)
	1399	1396	–COO^- symmetric and asymmetric stretching—peptidoglycan
1446	1427	1435	CH_2 and CH_3 deformations—lipids and proteins
	1503	1506	–C–C conjugated stretching—carotenoids
	1533	1557	Tryptophan; exopolysaccharides
	1598	1603	C–C ring stretching—phenylalanine, tyrosine and tryptophan
1659	1625	1654	C–O stretching (amide I); C–C stretching—lipids

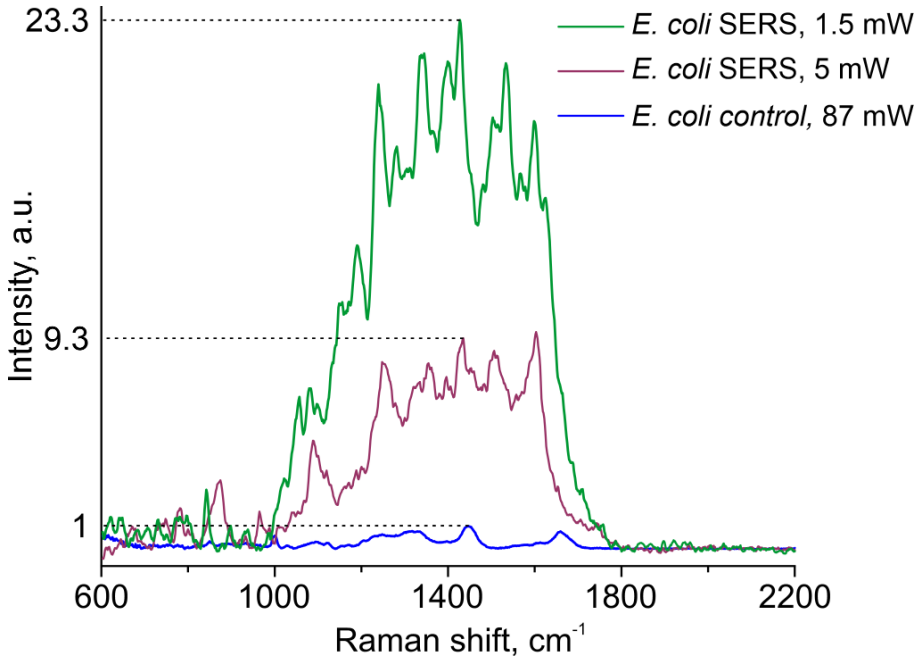

316

317 **Figure 5.** (a) SERS spectra of *E. coli* TOP10 obtained from microcapsules (blue). Normal Raman
318 spectrum of *E. coli*; (purple) and (green) are SERS spectra of *E. coli* immobilized on microcapsules
319 with laser power 5 mW and 1.5 mW, respectively.

320 In recent years, structural fabrication by nanoarchitectonics corresponds to the creation of a
321 rising tide in material design. Nanoarchitectonics has begun to spread into many fields and became
322 a common and basic concept, as seen in various applications such as nanostructured materials,
323 supramolecular assemblies, hybrid materials, fabrication methodologies.[89] LbL assemblies of
324 inorganic particle hybrid onto porous $CaCO_3$ particles achieved in this work and another
325 nanoarchitectonics-based work[30] by high precision deposition of alternating stacks of SiO_2 and
326 more densely packed TiO_2 nanoparticles are both using the cost-effective LbL process and opens
327 up possibilities in numerous technologically relevant applications.

328 **Conclusions**

329 Novel LbL inorganic microcapsules are designed using alternative adsorption of the gold
330 nanoparticles and in situ synthesis of the silver nanoparticles as layers. It is found in our work that
331 5 layers of metal nanoparticles is the minimum number of layers to form a stable shell. Such hollow

capsules keep the same spherical shape and size 4.25 ± 0.82 μm. The microcapsules are found to be efficient SERS substrates for a label-free detection of Rhodamine 6G. All types of the capsules reveal high enhancement factors in range of 10^6-10^7. The proof of principal of using such capsules for microorganism detection was shown by the bacteria immobilization on the particles surface. We demonstrate that the microcapsules provide sensitivity and 13 additional peaks related to the bacteria composition have been detected as well the enhancement of the major bacteria's peak $10^4/10^9$. We foresee that developed approaches would be feasible for the rapid diagnostics and discrimination of microorganisms particularly bacterial cells, which remains one of the most challenged tasks in health care, clinical, environmental, food field.

Appendix A. Supplementary material

Supplementary material.

Author Contributions

J.L. conducted research and wrote the manuscript, J.L. and D.K. conducted Raman measurements, A.L. contribute to bacteria experiments, D.V. contributed with working out the concept, B.V.P. supervised this work, A.G.S. supervised this work. All authors contributed to writing.

Declaration of Competing Interest

The authors declare no competing financial interest.

ACKNOWLEDGMENT

We acknowledge the support of European Commission (H2020-Twinning project "SurfBio", Grant No.: 952379). AGS acknowledges the Special Research Fund (BOF) of Ghent University

(01IO3618, BAS094-18, BOF14/IOP/003) and FWO (G043219, G043322N, I002620N). JL thanks the China Scholarship Council (CSC, 201908420257).

REFERENCES

[1] M. Delcea, H. Möhwald, A.G. Skirtach, Stimuli-responsive LbL capsules and nanoshells for drug delivery, Advanced Drug Delivery Reviews. 63 (2011) 730–747. https://doi.org/10.1016/j.addr.2011.03.010.

[2] E. Guzmán, R.G. Rubio, F. Ortega, A closer physico-chemical look to the Layer-by-Layer electrostatic self-assembly of polyelectrolyte multilayers, Advances in Colloid and Interface Science. 282 (2020) 102197. https://doi.org/10.1016/j.cis.2020.102197.

[3] A. Mateos-Maroto, I. Abelenda-Núñez, F. Ortega, R.G. Rubio, E. Guzmán, Polyelectrolyte Multilayers on Soft Colloidal Nanosurfaces: A New Life for the Layer-By-Layer Method, Polymers. 13 (2021) 1221. https://doi.org/10.3390/polym13081221.

[4] C. Déjugnat, D. Haložan, G.B. Sukhorukov, Defined Picogram Dose Inclusion and Release of Macromolecules using Polyelectrolyte Microcapsules, Macromolecular Rapid Communications. 26 (2005) 961–967. https://doi.org/10.1002/marc.200500121.

[5] T.M. Koller, M.H. Rausch, J. Ramos, P.S. Schulz, P. Wasserscheid, I.G. Economou, A.P. Fröba, Thermophysical Properties of the Ionic Liquids [EMIM][B(CN)4] and [HMIM][B(CN)4], J. Phys. Chem. B. 117 (2013) 8512–8523. https://doi.org/10.1021/jp400315h.

[6] D.V. Volodkin, N.I. Larionova, G.B. Sukhorukov, Protein Encapsulation via Porous CaCO3 Microparticles Templating, Biomacromolecules. 5 (2004) 1962–1972. https://doi.org/10.1021/bm049669e.

[7] B.V. Parakhonskiy, A.M. Yashchenok, M. Konrad, A.G. Skirtach, Colloidal micro- and nano-particles as templates for polyelectrolyte multilayer capsules, Advances in Colloid and Interface Science. 207 (2014) 253–264. https://doi.org/10.1016/j.cis.2014.01.022.

[8] R.J. Ono, A.L.Z. Lee, Z.X. Voo, S. Venkataraman, B.W. Koh, Y.Y. Yang, J.L. Hedrick, Biodegradable Strain-Promoted Click Hydrogels for Encapsulation of Drug-Loaded Nanoparticles and Sustained Release of Therapeutics, Biomacromolecules. 18 (2017) 2277–2285. https://doi.org/10.1021/acs.biomac.7b00377.

[9] X. Gu, Y. Wei, Q. Fan, H. Sun, R. Cheng, Z. Zhong, C. Deng, cRGD-decorated biodegradable polytyrosine nanoparticles for robust encapsulation and targeted delivery of doxorubicin to colorectal cancer in vivo, Journal of Controlled Release. 301 (2019) 110–118. https://doi.org/10.1016/j.jconrel.2019.03.005.

[10] G. Horvat, M. Pantić, Ž. Knez, Z. Novak, Encapsulation and drug release of poorly water soluble nifedipine from bio-carriers, Journal of Non-Crystalline Solids. 481 (2018) 486–493. https://doi.org/10.1016/j.jnoncrysol.2017.11.037.

[11] M. Kataria, K. Yadav, A. Nain, H.-I. Lin, H.-W. Hu, C.R. Paul Inbaraj, T.-J. Chang, Y.-M. Liao, H.-Y. Cheng, K.-H. Lin, H.-T. Chang, F.-G. Tseng, W.-H. Wang, Y.-F. Chen, Self-Sufficient and Highly Efficient Gold Sandwich Upconversion Nanocomposite Lasers for Stretchable and Bio-applications, ACS Appl. Mater. Interfaces. 12 (2020) 19840–19854. https://doi.org/10.1021/acsami.0c02602.

[12] T.V. Bukreeva, B.V. Parakhonsky, A.G. Skirtach, A.S. Susha, G.B. Sukhorukov, Preparation of polyelectrolyte microcapsules with silver and gold nanoparticles in a shell and the remote

destruction of microcapsules under laser irradiation, Crystallogr. Rep. 51 (2006) 863–869. https://doi.org/10.1134/S1063774506050178.
[13] B.V. Parakhonskiy, M.F. Bedard, T.V. Bukreeva, G.B. Sukhorukov, H. Möhwald, A.G. Skirtach, Nanoparticles on Polyelectrolytes at Low Concentration: Controlling Concentration and Size, J. Phys. Chem. C. 114 (2010) 1996–2002. https://doi.org/10.1021/jp904564v.
[14] L. Van der Meeren, J. Verduijn, J. Li, E. Verwee, D.V. Krysko, B.V. Parakhonskiy, A.G. Skirtach, Encapsulation of cells in gold nanoparticle functionalized hybrid Layer-by-Layer (LbL) hybrid shells – Remote effect of laser light, Applied Surface Science Advances. 5 (2021) 100111. https://doi.org/10.1016/j.apsadv.2021.100111.
[15] J.F. Liu, B. Jang, D. Issadore, A. Tsourkas, Use of magnetic fields and nanoparticles to trigger drug release and improve tumor targeting, WIREs Nanomedicine and Nanobiotechnology. 11 (2019) e1571. https://doi.org/10.1002/wnan.1571.
[16] M.-H. Chan, W. Chen, C.-H. Li, C.-Y. Fang, Y.-C. Chang, D.-H. Wei, R.-S. Liu, M. Hsiao, An Advanced In Situ Magnetic Resonance Imaging and Ultrasonic Theranostics Nanocomposite Platform: Crossing the Blood–Brain Barrier and Improving the Suppression of Glioblastoma Using Iron-Platinum Nanoparticles in Nanobubbles, ACS Appl. Mater. Interfaces. 13 (2021) 26759–26769. https://doi.org/10.1021/acsami.1c04990.
[17] A.G. Skirtach, B.G.D. Geest, A. Mamedov, A.A. Antipov, N.A. Kotov, G.B. Sukhorukov, Ultrasound stimulated release and catalysis using polyelectrolyte multilayer capsules, J. Mater. Chem. 17 (2007) 1050–1054. https://doi.org/10.1039/B609934C.
[18] M.V. Zyuzin, A.S. Timin, G.B. Sukhorukov, Multilayer Capsules Inside Biological Systems: State-of-the-Art and Open Challenges, Langmuir. 35 (2019) 4747–4762. https://doi.org/10.1021/acs.langmuir.8b04280.
[19] Q. Qiu, T. Liu, Z. Li, X. Ding, Facile synthesis of N-halamine-labeled silica–polyacrylamide multilayer core–shell nanoparticles for antibacterial ability, J. Mater. Chem. B. 3 (2015) 7203–7212. https://doi.org/10.1039/C5TB00973A.
[20] H. Gao, D. Wen, G.B. Sukhorukov, Composite silica nanoparticle/polyelectrolyte microcapsules with reduced permeability and enhanced ultrasound sensitivity, J. Mater. Chem. B. 3 (2015) 1888–1897. https://doi.org/10.1039/C4TB01717J.
[21] E.V. Lengert, S.I. Koltsov, J. Li, A.V. Ermakov, B.V. Parakhonskiy, E.V. Skorb, A.G. Skirtach, Nanoparticles in Polyelectrolyte Multilayer Layer-by-Layer (LbL) Films and Capsules—Key Enabling Components of Hybrid Coatings, Coatings. 10 (2020) 1131. https://doi.org/10.3390/coatings10111131.
[22] B.G.D. Geest, A.G. Skirtach, T.R.M.D. Beer, G.B. Sukhorukov, L. Bracke, W.R.G. Baeyens, J. Demeester, S.C.D. Smedt, Stimuli-Responsive Multilayered Hybrid Nanoparticle/Polyelectrolyte Capsules, Macromolecular Rapid Communications. 28 (2007) 88–95. https://doi.org/10.1002/marc.200600631.
[23] V. Sharma, A. Sundaramurthy, Reusable Hollow Polymer Microreactors Incorporated with Anisotropic Nanoparticles for Catalysis Application, ACS Omega. 4 (2019) 628–636. https://doi.org/10.1021/acsomega.8b02820.
[24] C.O. Nyapete, A.H.H. Benziger, S.W. Buckner, P.A. Jelliss, Fabrication and characterization of aluminum nanoparticles entrapped in hollow polymer capsules, Nano-Structures & Nano-Objects. 16 (2018) 282–287. https://doi.org/10.1016/j.nanoso.2018.07.009.
[25] N.A. Kotov, I. Dekany, J.H. Fendler, Layer-by-Layer Self-Assembly of Polyelectrolyte-Semiconductor Nanoparticle Composite Films, J. Phys. Chem. 99 (1995) 13065–13069. https://doi.org/10.1021/j100035a005.

[26] C.Q. Peng, Y.S. Thio, R.A. Gerhardt, Conductive paper fabricated by layer-by-layer assembly of polyelectrolytes and ITO nanoparticles, Nanotechnology. 19 (2008) 505603. https://doi.org/10.1088/0957-4484/19/50/505603.
[27] Y. Chaikin, H. Leader, R. Popovitz-Biro, A. Vaskevich, I. Rubinstein, Versatile Scheme for the Step-by-Step Assembly of Nanoparticle Multilayers, Langmuir. 27 (2011) 1298–1307. https://doi.org/10.1021/la103913u.
[28] Z. Liu, Z. Yan, L. Bai, Layer-by-layer assembly of polyelectrolyte and gold nanoparticle for highly reproducible and stable SERS substrate, Applied Surface Science. 360 (2016) 437–441. https://doi.org/10.1016/j.apsusc.2015.09.151.
[29] H. Li, Z. Li, L. Wu, Y. Zhang, M. Yu, L. Wei, Constructing Metal Nanoparticle Multilayers with Polyphenylene Dendrimer/Gold Nanoparticles via "Click" Chemistry, Langmuir. 29 (2013) 3943–3949. https://doi.org/10.1021/la400397q.
[30] P. Kurt, D. Banerjee, R.E. Cohen, M.F. Rubner, Structural color via layer-by-layer deposition: layered nanoparticle arrays with near-UV and visible reflectivity bands, J. Mater. Chem. 19 (2009) 8920–8927. https://doi.org/10.1039/B912211G.
[31] R.G. Freeman, K.C. Grabar, K.J. Allison, R.M. Bright, J.A. Davis, A.P. Guthrie, M.B. Hommer, M.A. Jackson, P.C. Smith, D.G. Walter, M.J. Natan, Self-Assembled Metal Colloid Monolayers: An Approach to SERS Substrates, Science. 267 (1995) 1629–1632. https://doi.org/10.1126/science.267.5204.1629.
[32] S. Bernard, N. Felidj, S. Truong, P. Peretti, G. Lévi, J. Aubard, Study of Langmuir–Blodgett phospholipidic films deposited on surface enhanced Raman scattering active gold nanoparticle monolayers, Biopolymers. 67 (2002) 314–318. https://doi.org/10.1002/bip.10086.
[33] R.F. Aroca, P.J.G. Goulet, dos Santos David S., R.A. Alvarez-Puebla, O.N. Oliveira, Silver Nanowire Layer-by-Layer Films as Substrates for Surface-Enhanced Raman Scattering, Anal. Chem. 77 (2005) 378–382. https://doi.org/10.1021/ac048806v.
[34] C. Peng, Y. Song, G. Wei, W. Zhang, Z. Li, W.-F. Dong, Self-assembly of λ-DNA networks/Ag nanoparticles: Hybrid architecture and active-SERS substrate, Journal of Colloid and Interface Science. 317 (2008) 183–190. https://doi.org/10.1016/j.jcis.2007.09.017.
[35] B.P. Binks, Colloidal Particles at a Range of Fluid–Fluid Interfaces, Langmuir. 33 (2017) 6947–6963. https://doi.org/10.1021/acs.langmuir.7b00860.
[36] M. A. Khan, M. F. Haase, Stabilizing liquid drops in nonequilibrium shapes by the interfacial crosslinking of nanoparticles, Soft Matter. 17 (2021) 2034–2041. https://doi.org/10.1039/D0SM02120B.
[37] A. Mateos-Maroto, L. Fernández-Peña, I. Abelenda-Núñez, F. Ortega, R.G. Rubio, E. Guzmán, Polyelectrolyte Multilayered Capsules as Biomedical Tools, Polymers. 14 (2022) 479. https://doi.org/10.3390/polym14030479.
[38] L. Van der Meeren, J. Li, B.V. Parakhonskiy, D.V. Krysko, A.G. Skirtach, Classification of analytics, sensorics, and bioanalytics with polyelectrolyte multilayer capsules, Anal Bioanal Chem. 412 (2020) 5015–5029. https://doi.org/10.1007/s00216-020-02428-8.
[39] R. Xiong, S.J. Soenen, K. Braeckmans, A.G. Skirtach, Towards Theranostic Multicompartment Microcapsules: in-situ Diagnostics and Laser-induced Treatment, Theranostics. 3 (2013) 141–151. https://doi.org/10.7150/thno.5846.
[40] T. Xie, C. Jing, Y.-T. Long, Single plasmonic nanoparticles as ultrasensitive sensors, Analyst. 142 (2017) 409–420. https://doi.org/10.1039/C6AN01852A.

[41] M. Kamran, M. Haroon, S.A. Popoola, A.R. Almohammedi, A.A. Al-Saadi, T.A. Saleh, Characterization of valeric acid using substrate of silver nanoparticles with SERS, Journal of Molecular Liquids. 273 (2019) 536–542. https://doi.org/10.1016/j.molliq.2018.10.037.
[42] N. Pazos-Pérez, W. Ni, A. Schweikart, R. A. Alvarez-Puebla, A. Fery, L. M. Liz-Marzán, Highly uniform SERS substrates formed by wrinkle-confined drying of gold colloids, Chemical Science. 1 (2010) 174–178. https://doi.org/10.1039/C0SC00132E.
[43] K. Kneipp, H. Kneipp, J. Kneipp, Surface-Enhanced Raman Scattering in Local Optical Fields of Silver and Gold NanoaggregatesFrom Single-Molecule Raman Spectroscopy to Ultrasensitive Probing in Live Cells, Acc. Chem. Res. 39 (2006) 443–450. https://doi.org/10.1021/ar050107x.
[44] K. Hering, D. Cialla, K. Ackermann, T. Dörfer, R. Möller, H. Schneidewind, R. Mattheis, W. Fritzsche, P. Rösch, J. Popp, SERS: a versatile tool in chemical and biochemical diagnostics, Anal Bioanal Chem. 390 (2008) 113–124. https://doi.org/10.1007/s00216-007-1667-3.
[45] B.V. Parakhonskiy, A. Abalymov, A. Ivanova, D. Khalenkow, A.G. Skirtach, Magnetic and silver nanoparticle functionalized calcium carbonate particles—Dual functionality of versatile, movable delivery carriers which can surface-enhance Raman signals, Journal of Applied Physics. 126 (2019) 203102. https://doi.org/10.1063/1.5111973.
[46] R. Kamyshinsky, I. Marchenko, B. Parakhonskiy, A. Yashchenok, Y. Chesnokov, A. Mikhutkin, D. Gorin, A. Vasiliev, T. Bukreeva, Composite materials based on Ag nanoparticles in situ synthesized on the vaterite porous matrices, Nanotechnology. 30 (2018) 035603. https://doi.org/10.1088/1361-6528/aaea38.
[47] B.V. Parakhonskiy, Yu.I. Svenskaya, A.M. Yashchenok, H.A. Fattah, O.A. Inozemtseva, F. Tessarolo, R. Antolini, D.A. Gorin, Size controlled hydroxyapatite and calcium carbonate particles: Synthesis and their application as templates for SERS platform, Colloids and Surfaces B: Biointerfaces. 118 (2014) 243–248. https://doi.org/10.1016/j.colsurfb.2014.03.053.
[48] A.M. Yashchenok, D. Borisova, B.V. Parakhonskiy, A. Masic, B. Pinchasik, H. Möhwald, A.G. Skirtach, Nanoplasmonic smooth silica versus porous calcium carbonate bead biosensors for detection of biomarkers, Annalen Der Physik. 524 (2012) 723–732. https://doi.org/10.1002/andp.201200158.
[49] E. Lengert, M. Saveleva, A. Abalymov, V. Atkin, P.C. Wuytens, R. Kamyshinsky, A.L. Vasiliev, D.A. Gorin, G.B. Sukhorukov, A.G. Skirtach, B. Parakhonskiy, Silver Alginate Hydrogel Micro- and Nanocontainers for Theranostics: Synthesis, Encapsulation, Remote Release, and Detection, ACS Appl. Mater. Interfaces. 9 (2017) 21949–21958. https://doi.org/10.1021/acsami.7b08147.
[50] E. Lengert, B. Parakhonskiy, D. Khalenkow, A. Zečić, M. Vangheel, J.M.M. Moreno, B. P. Braeckman, A. G. Skirtach, Laser-induced remote release in vivo in C. elegans from novel silver nanoparticles-alginate hydrogel shells, Nanoscale. 10 (2018) 17249–17256. https://doi.org/10.1039/C8NR00893K.
[51] R. Ahijado-Guzmán, P. Gómez-Puertas, R.A. Alvarez-Puebla, G. Rivas, L.M. Liz-Marzán, Surface-Enhanced Raman Scattering-Based Detection of the Interactions between the Essential Cell Division FtsZ Protein and Bacterial Membrane Elements, ACS Nano. 6 (2012) 7514–7520. https://doi.org/10.1021/nn302825u.

[52] M. Gellner, S. Niebling, H. Y. Kuchelmeister, C. Schmuck, S. Schlücker, Plasmonically active micron-sized beads for integrated solid-phase synthesis and label-free SERS analysis, Chemical Communications. 47 (2011) 12762–12764. https://doi.org/10.1039/C1CC13562G.
[53] X. Yang, S. Wang, Y. Wang, Y. He, Y. Chai, R. Yuan, Stimuli-Responsive DNA Microcapsules for SERS Sensing of Trace MicroRNA, ACS Appl. Mater. Interfaces. 10 (2018) 12491–12496. https://doi.org/10.1021/acsami.8b01974.
[54] A. Quinn, Y.-H. You, M.J. McShane, Hydrogel Microdomain Encapsulation of Stable Functionalized Silver Nanoparticles for SERS pH and Urea Sensing, Sensors. 19 (2019) 3521. https://doi.org/10.3390/s19163521.
[55] L. Bi, Y. Wang, Y. Yang, Y. Li, S. Mo, Q. Zheng, L. Chen, Highly Sensitive and Reproducible SERS Sensor for Biological pH Detection Based on a Uniform Gold Nanorod Array Platform, ACS Appl. Mater. Interfaces. 10 (2018) 15381–15387. https://doi.org/10.1021/acsami.7b19347.
[56] I.Y. Stetciura, A.V. Markin, A.N. Ponomarev, A.V. Yakimansky, T.S. Demina, C. Grandfils, D.V. Volodkin, D.A. Gorin, New Surface-Enhanced Raman Scattering Platforms: Composite Calcium Carbonate Microspheres Coated with Astralen and Silver Nanoparticles, Langmuir. 29 (2013) 4140–4147. https://doi.org/10.1021/la305117t.
[57] A. Yashchenok, A. Masic, D. Gorin, B.S. Shim, N.A. Kotov, P. Fratzl, H. Möhwald, A. Skirtach, Nanoengineered Colloidal Probes for Raman-based Detection of Biomolecules inside Living Cells, Small. 9 (2013) 351–356. https://doi.org/10.1002/smll.201201494.
[58] N. Turk, A. Raza, P. Wuytens, H. Demol, M. Van Daele, C. Detavernier, A. Skirtach, K. Gevaert, R. Baets, Comparison of Free-Space and Waveguide-Based SERS Platforms, Nanomaterials. 9 (2019) 1401. https://doi.org/10.3390/nano9101401.
[59] A. Csaki, F. Jahn, I. Latka, T. Henkel, D. Malsch, T. Schneider, K. Schröder, K. Schuster, A. Schwuchow, R. Spittel, D. Zopf, W. Fritzsche, Nanoparticle Layer Deposition for Plasmonic Tuning of Microstructured Optical Fibers, Small. 6 (2010) 2584–2589. https://doi.org/10.1002/smll.201001071.
[60] M. Saveleva, E. Prikhozhdenko, D. Gorin, A.G. Skirtach, A. Yashchenok, B. Parakhonskiy, Polycaprolactone-Based, Porous CaCO3 and Ag Nanoparticle Modified Scaffolds as a SERS Platform With Molecule-Specific Adsorption, Front. Chem. 7 (2020). https://doi.org/10.3389/fchem.2019.00888.
[61] S. Hong, T. Chen, Y. Zhu, A. Li, Y. Huang, X. Chen, Live-Cell Stimulated Raman Scattering Imaging of Alkyne-Tagged Biomolecules, Angewandte Chemie. 126 (2014) 5937–5941. https://doi.org/10.1002/ange.201400328.
[62] E.A. Vitol, Z. Orynbayeva, G. Friedman, Y. Gogotsi, Nanoprobes for intracellular and single cell surface-enhanced Raman spectroscopy (SERS), Journal of Raman Spectroscopy. 43 (2012) 817–827. https://doi.org/10.1002/jrs.3100.
[63] C. Krafft, M. Schmitt, I.W. Schie, D. Cialla-May, C. Matthäus, T. Bocklitz, J. Popp, Label-Free Molecular Imaging of Biological Cells and Tissues by Linear and Nonlinear Raman Spectroscopic Approaches, Angewandte Chemie International Edition. 56 (2017) 4392–4430. https://doi.org/10.1002/anie.201607604.
[64] X. Jin, B.N. Khlebtsov, V.A. Khanadeev, N.G. Khlebtsov, J. Ye, Rational Design of Ultrabright SERS Probes with Embedded Reporters for Bioimaging and Photothermal Therapy, ACS Appl. Mater. Interfaces. 9 (2017) 30387–30397. https://doi.org/10.1021/acsami.7b08733.

[65] N. Bontempi, L. Carletti, C.D. Angelis, I. Alessandri, Plasmon-free SERS detection of environmental CO2 on TiO2 surfaces, Nanoscale. 8 (2016) 3226–3231. https://doi.org/10.1039/C5NR08380J.
[66] A. Mariño-Lopez, A. Sousa-Castillo, M. Blanco-Formoso, L.N. Furini, L. Rodríguez-Lorenzo, N. Pazos-Perez, L. Guerrini, M. Pérez-Lorenzo, M.A. Correa-Duarte, R.A. Alvarez-Puebla, Microporous Plasmonic Capsules as Stable Molecular Sieves for Direct SERS Quantification of Small Pollutants in Natural Waters, ChemNanoMat. 5 (2019) 46–50. https://doi.org/10.1002/cnma.201800355.
[67] D. Ma, C. Huang, J. Zheng, J. Tang, J. Li, J. Yang, R. Yang, Quantitative detection of exosomal microRNA extracted from human blood based on surface-enhanced Raman scattering, Biosensors and Bioelectronics. 101 (2018) 167–173. https://doi.org/10.1016/j.bios.2017.08.062.
[68] J.C. Fraire, S. Stremersch, D. Bouckaert, T. Monteyne, T. De Beer, P. Wuytens, R. De Rycke, A.G. Skirtach, K. Raemdonck, S. De Smedt, K. Braeckmans, Improved Label-Free Identification of Individual Exosome-like Vesicles with Au@Ag Nanoparticles as SERS Substrate, ACS Appl. Mater. Interfaces. 11 (2019) 39424–39435. https://doi.org/10.1021/acsami.9b11473.
[69] J. Wang, Y.-C. Kao, Q. Zhou, A. Wuethrich, M.S. Stark, H. Schaider, H.P. Soyer, L.L. Lin, M. Trau, An Integrated Microfluidic-SERS Platform Enables Sensitive Phenotyping of Serum Extracellular Vesicles in Early Stage Melanomas, Advanced Functional Materials. n/a (n.d.) 2010296. https://doi.org/10.1002/adfm.202010296.
[70] E.S. Prikhozhdenko, V.S. Atkin, B.V. Parakhonskiy, I.A. Rybkin, A. Lapanje, G.B. Sukhorukov, D.A. Gorin, A.M. Yashchenok, New post-processing method of preparing nanofibrous SERS substrates with a high density of silver nanoparticles, RSC Adv. 6 (2016) 84505–84511. https://doi.org/10.1039/C6RA18636J.
[71] E. Lengert, A.M. Yashchenok, V. Atkin, A. Lapanje, D.A. Gorin, G.B. Sukhorukov, B.V. Parakhonskiy, Hollow silver alginate microspheres for drug delivery and surface enhanced Raman scattering detection, RSC Adv. 6 (2016) 20447–20452. https://doi.org/10.1039/C6RA02019D.
[72] C. Fan, Z. Hu, A. Mustapha, M. Lin, Rapid detection of food- and waterborne bacteria using surface-enhanced Raman spectroscopy coupled with silver nanosubstrates, Appl Microbiol Biotechnol. 92 (2011) 1053–1061. https://doi.org/10.1007/s00253-011-3634-3.
[73] C.S. Peyratout, L. Dähne, Tailor-Made Polyelectrolyte Microcapsules: From Multilayers to Smart Containers, Angewandte Chemie International Edition. 43 (2004) 3762–3783. https://doi.org/10.1002/anie.200300568.
[74] D.I. Gittins, F. Caruso, Spontaneous Phase Transfer of Nanoparticulate Metals from Organic to Aqueous Media, Angewandte Chemie International Edition. 40 (2001) 3001–3004. https://doi.org/10.1002/1521-3773(20010817)40:16<3001::AID-ANIE3001>3.0.CO;2-5.
[75] D.V. Volodkin, A.I. Petrov, M. Prevot, G.B. Sukhorukov, Matrix Polyelectrolyte Microcapsules: New System for Macromolecule Encapsulation, Langmuir. 20 (2004) 3398–3406. https://doi.org/10.1021/la036177z.
[76] B. V. Parakhonskiy, C. Foss, E. Carletti, M. Fedel, A. Haase, A. Motta, C. Migliaresi, R. Antolini, Tailored intracellular delivery via a crystal phase transition in 400 nm vaterite particles, Biomaterials Science. 1 (2013) 1273–1281. https://doi.org/10.1039/C3BM60141B.

[77] L. Zhang, X. Ren, Y. Zhang, K. Zhang, Step-Growth Polymerization Method for Ultrahigh Molecular Weight Polymers, ACS Macro Lett. 8 (2019) 948–954. https://doi.org/10.1021/acsmacrolett.9b00475.
[78] M. Lafuente, I. Pellejero, V. Sebastián, M.A. Urbiztondo, R. Mallada, M.P. Pina, J. Santamaría, Highly sensitive SERS quantification of organophosphorous chemical warfare agents: A major step towards the real time sensing in the gas phase, Sensors and Actuators B: Chemical. 267 (2018) 457–466. https://doi.org/10.1016/j.snb.2018.04.058.
[79] Y. Mandelbaum, R. Mottes, Z. Zalevsky, D. Zitoun, A. Karsenty, Investigations of Shape, Material and Excitation Wavelength Effects on Field Enhancement in SERS Advanced Tips, Nanomaterials. 11 (2021) 237. https://doi.org/10.3390/nano11010237.
[80] K. Hamasha, Q.I. Mohaidat, R.A. Putnam, R.C. Woodman, S. Palchaudhuri, S.J. Rehse, Sensitive and specific discrimination of pathogenic and nonpathogenic Escherichia coli using Raman spectroscopy—a comparison of two multivariate analysis techniques, Biomed. Opt. Express, BOE. 4 (2013) 481–489. https://doi.org/10.1364/BOE.4.000481.
[81] M. Harz, P. Rösch, K.-D. Peschke, O. Ronneberger, H. Burkhardt, J. Popp, Micro-Raman spectroscopic identification of bacterial cells of the genus Staphylococcus and dependence on their cultivation conditions, Analyst. 130 (2005) 1543–1550. https://doi.org/10.1039/B507715J.
[82] W.E. Huang, R.I. Griffiths, I.P. Thompson, M.J. Bailey, A.S. Whiteley, Raman Microscopic Analysis of Single Microbial Cells, Anal. Chem. 76 (2004) 4452–4458. https://doi.org/10.1021/ac049753k.
[83] K.C. Schuster, E. Urlaub, J.R. Gapes, Single-cell analysis of bacteria by Raman microscopy: spectral information on the chemical composition of cells and on the heterogeneity in a culture, Journal of Microbiological Methods. 42 (2000) 29–38. https://doi.org/10.1016/S0167-7012(00)00169-X.
[84] F.S. de S. Oliveira, H.E. Giana, L.S. Jr, Discrimination of selected species of pathogenic bacteria using near-infrared Raman spectroscopy and principal components analysis, JBO. 17 (2012) 107004. https://doi.org/10.1117/1.JBO.17.10.107004.
[85] W.E. Huang, M.J. Bailey, I.P. Thompson, A.S. Whiteley, A.J. Spiers, Single-Cell Raman Spectral Profiles of Pseudomonas fluorescens SBW25 Reflects in vitro and in planta Metabolic History, Microb Ecol. 53 (2007) 414–425. https://doi.org/10.1007/s00248-006-9138-5.
[86] L. Silveira, B. Bodanese, R.A. Zângaro, M.T.T. Pacheco, Discrete Wavelet Transform for Denoising Raman Spectra of Human Skin Tissues Used in a Discriminant Diagnostic Algorithm, Instrumentation Science & Technology. 38 (2010) 268–282. https://doi.org/10.1080/10739149.2010.508318.
[87] V. Ciobotă, E.-M. Burkhardt, W. Schumacher, P. Rösch, K. Küsel, J. Popp, The influence of intracellular storage material on bacterial identification by means of Raman spectroscopy, Anal Bioanal Chem. 397 (2010) 2929–2937. https://doi.org/10.1007/s00216-010-3895-1.
[88] G. Naja, P. Bouvrette, S. Hrapovic, J.H.T. Luong, Raman-based detection of bacteria using silver nanoparticles conjugated with antibodies, Analyst. 132 (2007) 679–686. https://doi.org/10.1039/B701160A.
[89] M. Aono, K. Ariga, The Way to Nanoarchitectonics and the Way of Nanoarchitectonics, Advanced Materials. 28 (2016) 989–992. https://doi.org/10.1002/adma.201502868.

666

Supporting Information

Surface enhanced Raman scattering (SERS) enhancement by layer-by-layer (LbL) assembly all-nanoparticle microcapsules

Jie Li,[a] Dmitry Khalenkow,[a] Dmitry Volodkin,[b] Ales Lapanje,[c] Andre G. Skirtach,[a] and Bogdan V. Parakhonskiy[a]*

a. Bio-Nanotechnology Laboratory, Faculty of Bioscience Engineering, Ghent University, 9000, Belgium.

b. Department of Chemistry and Forensics, School of Science and Technology, Nottingham Trent University, Clifton Lane, Nottingham NG11 8NS, UK.

c. Department of Environmental Sciences, Jozef Stefan Institute, Jamova cesta 39, 1000 Ljubljana, Slovenia

Corresponding author's E-mail: jiejieli.li@ugent.be.

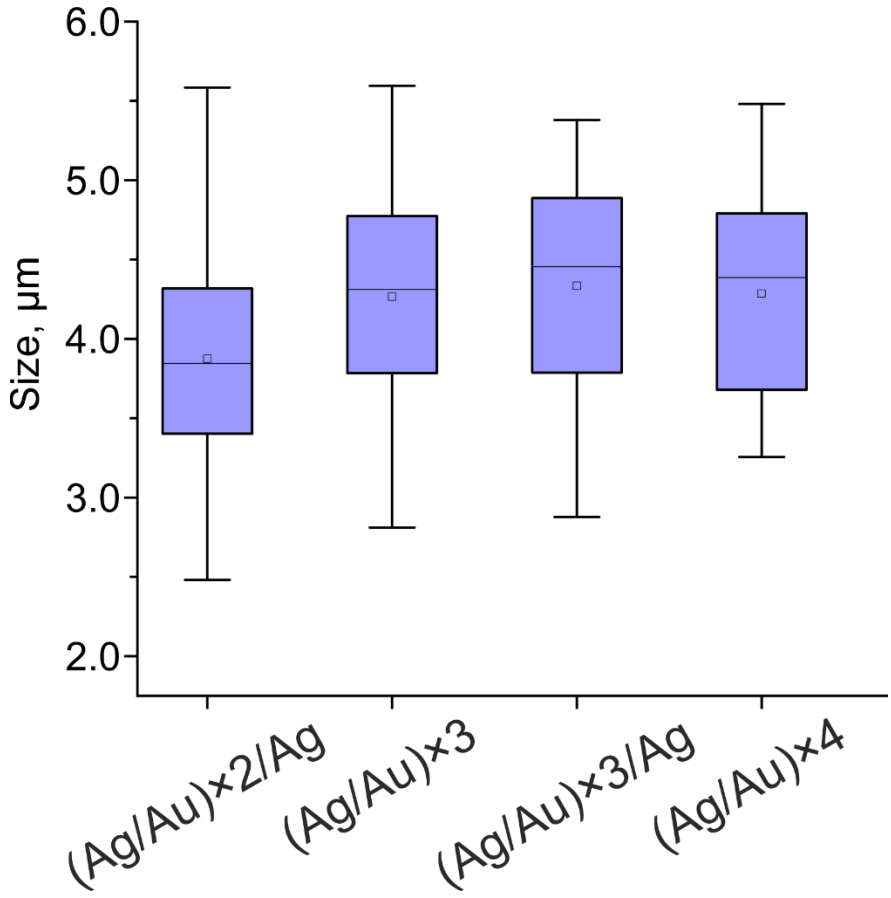

682
683

684 Fig. S1. Size of microcapsules with different layers of shell.

685